Journal of Applied Fluid Mechanics, Vol. 19, No. 1, pp. 3398-3414, 2026. Available online at <a href="www.jafmonline.net">www.jafmonline.net</a>, ISSN 1735-3572, EISSN 1735-3645. <a href="https://doi.org/10.47176/jafm.19.1.3580">https://doi.org/10.47176/jafm.19.1.3580</a>



# Multi-objective Optimization Design for Reversible Counter-rotating Axial Flow Pump Based on the Adaptive Modified Genetic Algorithm

Q. Xiang<sup>1</sup>, D. Kong<sup>1</sup>, W. Xu<sup>2</sup>, X. Wang<sup>1</sup>, Y. Xie<sup>1</sup>, and Y. Zhao<sup>3†</sup>

Research Center of Fluid Machinery Engineering and Technology, Jiangsu University, Zhenjiang 212013, China
School of Energy and Power Engineering, Jiangsu University, Zhenjiang 212013, Jiangsu Province, China
School of the Environment and Safety Engineering, Jiangsu University, Zhenjiang, 212013, China

†Corresponding Author Email: ujszyy@ujs.edu.cn

#### **ABSTRACT**

Conventional hydraulic design methodologies for reversible counter-rotating axial flow pumps predominantly adhere to traditional axial flow pump design principles. However, existing optimization approaches inadequately analyze the individual design parameters, their synergistic interactions, and relative contributions, leading to suboptimal pump efficiency and compromised bidirectional multi-objective operational performance. To overcome these limitations, this study proposes a surrogate model-based framework integrated with an automated optimization platform developed in Isight software. A comprehensive evaluation of 120 simulated sample points is conducted to quantify the effects of geometric parameters on hydraulic performance. The adaptive modified genetic algorithm (AMGA) is employed to maximize operational efficiency through systematic impeller parameter optimization within the design space, while satisfying predefined pump specifications. Sensitivity analysis identified the angle of attack as the most influential parameter, accounting for 51.28% and 56.2% of the total variance in head and efficiency, respectively. Post-optimization results demonstrated a 3% increase in simulated efficiency at the design operating point, accompanied by a 14.5 kW reduction in shaft power consumption. These findings establish a robust foundation for advancing the multi-objective design optimization of reversible counter-rotating axial flow pumps.

#### Article History

Received April 8, 2025 Revised August 14, 2025 Accepted August 15, 2025 Available online November 5, 2025

#### Keywords:

Reversible counter-rotating axial flow pump
S-shaped airfoil
Optimization design
Proxy models
Adaptive multi-objective genetic algorithm (AMGA)

#### 1. INTRODUCTION

Axial flow pumps are critical components in hydraulic engineering systems, including agricultural irrigation and urban water management, owing to their high volumetric flow capacity. Nevertheless, when operating in reverse-rotation mode, these pumps demonstrate suboptimal efficiency accompanied by substantial energy dissipation. To address the demand for bidirectional fluid transfer, reversible counter-rotating axial flow pumps have been introduced. Featuring a symmetrically designed impeller, these pumps enable dual-directional operation through motor rotation reversal (Harris et al., 2020), rendering them ideal for riverine and coastal pumping stations requiring alternating irrigation and drainage cycles. Distinct from conventional axial flow pumps, reversible counter-rotating axial flow pumps multifunctional advantages: structural compactness, minimized spatial footprint, cost-effective

construction, extended efficiency ranges, operational stability, and simplified maintenance protocols. These attributes have driven their widespread adoption in tidal energy systems, marine propulsion, and hydraulic infrastructure. Furthermore, their unique bidirectional capability - efficient operation in both pump and turbine modes - has positioned reversible counter-rotating axial flow pumps as a prominent research focus in fluid machinery. Despite these advancements, emerging Current challenges persist. hydraulic methodologies for reversible counter-rotating axial flow pumps predominantly replicate conventional axial flow pump frameworks (Hoffstaedt et al., 2022), leading to frequently observed discrepancies between achieved and anticipated operational efficiencies.

Reversible counter-rotating axial flow pumps represent an advanced variant of axial flow pumps. Unlike conventional designs utilizing fixed guide vanes (Ma & Wang, 2017; Shi et al., 2015), these pumps incorporate S-

NOMENCLATURE								
α	attack angle	P	shaft power					
LT	cascade density at the impeller rim	DOE	Design of Experiment					
N	root and cascade density multiplier	NPSHr	Net Positive Suction Head Required					
S	axial interstage gap	Eff	efficiency of the pump					
LT@high/low	LT at a high/low level	$\rho$	the density of water					
N@high/low	N at a high/low level	$S_{i}$	the regression coefficients					
S@high/low	S at a high/low level							

shaped impellers with bidirectional functionality, enabling equivalent hydraulic performance in both forward and reverse operational modes (Xie et al., 2022; Fahlbeck et al., 2021; Vashahi et al., 2017). The distinctive two-stage impeller configuration directs fluid sequentially through the primary and secondary impellers. While this architecture enhances pump head and cavitation resistance (Zhang et al., 2020a), the absence of systematic hydraulic optimization for inter-stage flow dynamics and parametric design frequently results in suboptimal overall efficiency, ultimately compromising practical performance. Recent investigations have advanced understanding of these systems. An et al. (2023) performed computational fluid dynamics (CFD) simulations to evaluate blade count effects on pump-mode performance, elucidating mechanisms governing tip leakage vortices, wake interactions. and leading-edge flow impacts downstream impellers. Chen et al. (2023) demonstrated that blade angle modifications substantially alter internal flow patterns and hydraulic characteristics, particularly vortex formation at trailing impellers. Xiuli et al. (2020) established correlations between inter-stage clearance dimensions and critical performance metrics (head, efficiency) through parametric hydraulic design of S-blade configurations. The inherent complexity of reversible counter-rotating axial flow pump design necessitates comprehensive consideration of inter-stage matching and hydrodynamic interference (Kan et al., Consequently, single-objective optimization approaches prove inadequate. To achieve further efficiency improvements, a systematic optimization framework must be implemented that accounts for parameter interactions, relative contribution weights, and multi-objective operational constraints.

The evolution of turbomachinery design optimization progressed substantially with advances computational technology and maturation of optimization theory, evolving from conventional gradient-based approaches to advanced machine learning (ML) methodologies. This paradigm shift has been propelled by enhanced computational power and refined understanding of fluid-structure interactions. Modern frameworks effectively coordinate multiple design parameters and constraints while optimizing critical performance metrics, including efficiency, pressure ratio, and structural integrity. The research paradigm has consequently shifted from single to multi-objective optimization, which enables concurrent resolution of conflicting objectives through Pareto-optimal solution sets. Dominance criteria serve as principal evaluators of solution quality, exemplified by Sharma & Kumar (2022) application of the elite nondominated sorting genetic algorithm-II (NSGA-II) to optimize a two-stage LNG cryogenic submerged pump. Wang et al. (2022), aiming to minimize energy loss and optimize suction performance under the 0.7 Q operating condition. Post-optimization, the active suppression of impinging flow, diverging flow, and rotating stall in the two-stage impeller reduced the total entropy generation rate by 6.18%, while the pump head decreased by only 1.25%. Kim et al. (2016) combined a hybrid multiobjective genetic algorithm with an agent model based on Latin Hypercube Sampling, optimizing the hub and tip blade angles of the two-stage impeller, resulting in pump efficiency improvements of 0.80% and 1.02%, and turbine efficiency improvements of 0.50% and 0.27%, respectively. Zhang et al. (2020b) proposed a rotational speed control method for the front and rear rotors, significantly enhancing the performance of counterrotating axial flow pumps across a wide flow rate range and optimizing energy efficiency through a fast and effective performance prediction model. Kim et al. (2018) used the hub and tip blade angles of the rear impeller in the counter-rotating pump turbine as design variables, combining efficiency and weighting factors into a single objective function, and optimized using Latin Hypercube Sampling and radial basis neural network agent models. Post-optimization, the pump and turbine mode efficiencies increased by 1.01% and 0.52%, respectively, though the turbine mode flow rate is reduced. Hu et al. (2023) proposed a multi-objective optimization strategy for impellers with a broader operating range, optimizing blade control parameters and revealing the relationship between geometric characteristics and performance, particularly the effects of blade loading and blade tilt angle on efficiency, cavitation resistance, and stability. Postoptimization, the peak pump efficiency increased by 0.45%, the NPSHr by 0.36 m, and the rated turbine efficiency increased by 0.12%. Gao et al. (2018) applied bi-objective and tri-objective optimization methods for hydraulic optimization of the inlet and outlet diffusion sections of a pumped storage plant, generating an approximation function through Response Surface Methodology (RSM) and using the Non-dominated Sorting Genetic Algorithm (NSGA-II) to perform optimization (Xu et al., 2019; Huang et al., 2023). The head loss is reduced by 2.71%, the velocity nonuniformity by 21.05%, and the discharge non-uniformity by 2.24%. Qin et al. (2022) introduced the concepts of 'swept', 'curved (inclined)', and 'twisted', proposing nine parameters to control the geometry of the high-pressure side and establishing a multi-objective optimal design system based on the DOE (Design of Experiment) process. The efficiency of the optimized impeller increased by 1.17% and 0.46% in pump mode and turbine mode,

respectively. Mansour et al. (2022) employed a multiobjective optimization approach to determine the optimal configuration of two mixed-phase liquids flowing in a spiral tube, utilizing the Flow Optimization Library (OPAL) to automate the numerical simulation process and derive a correlation between the predicted pressure drop and mixing coefficients, achieving optimal simultaneous optimization of mixing efficiency and minimum pump power.

Current multi-objective optimization studies for reversible counter-rotating axial flow pumps exhibit two critical limitations: (1) insufficient systematic analysis of individual parameter impacts, synergistic interactions, and relative contribution weights on hydraulic performance, leading to constrained efficiency gains post-optimization. (2) inadequate experimental validation of pre- and postoptimization impeller configurations. To bridge these gaps, this study establishes an integrated framework combining parametric optimization with experimental verification. To meet the design requirements of the pump and maximize the efficiency, this study is based on the DOE design, selecting four parameterized variables: attack angle ( $\alpha$ ), cascade density at the impeller rim (LT), root and cascade density multiplier (N), axial interstage gap (S), These variables are analyzed in terms of their main effects, interaction effects, and contribution rates to reveal their influence on performance characteristics. Employing computational fluid dynamics (CFD) simulations coupled with the adaptive multi-objective genetic algorithm (AMGA), we executed global optimization within the design space under constrained head requirements. Finally, the performance improvement before and after optimization is validated through experiments. This systematic approach demonstrates significant potential for advancing the hydraulic performance ceiling of bidirectional pump systems.

#### 2. MODEL AND METHODS

#### 2.1 Geometric Modeling

The reversible counter-rotating axial flow pump distinguishes itself from conventional reversible axial flow pumps through its innovative dual-stage impeller configuration. While traditional reversible pumps achieve reverse operation by inverting a unidirectional impeller, the present design replaces the rear guide vane with a second-stage counter-rotating impeller. This study focuses on a blade profile featuring a symmetrically reversed S-shaped airfoil, engineered to maintain consistent hydraulic performance across bidirectional flow conditions.

Parametric modelling is achieved by using MATLAB outputs and is modelled by CFturbo. As shown in Fig. 1, the computational domain encompasses five critical components to enable precise characterization of parametric effects on hydraulic performance and internal flow dynamics: inlet section, first-stage impeller, interstage gap, second-stage impeller, and outlet section.

The inlet and outlet sections are configured with 4D pipe lengths to ensure flow field stabilization and computational accuracy at boundary conditions. Key

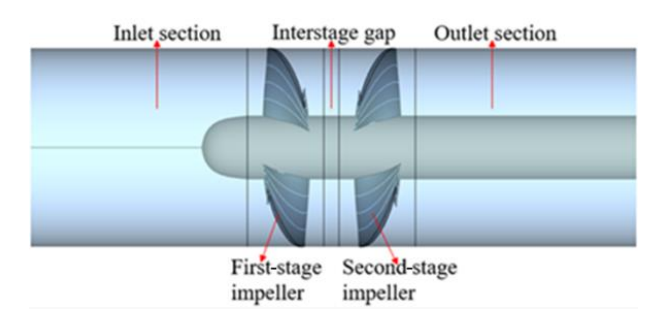


Fig. 1 3D model of reversible counter-rotating axial flow pump

Table 1 Main parameters of the impeller

Parameter	Symbol	Value
Flow rate (m³/h)	Q	21600
Design head (m)	$H_d$	5.3
Rotational speed (r/min)	$n_d$	300
Hub diameter (mm)	$d_{ m h}$	416
Number of blades	Z	3
Impeller diameter (mm)	D	1300
Design interstage gap (mm)	$S_d$	220

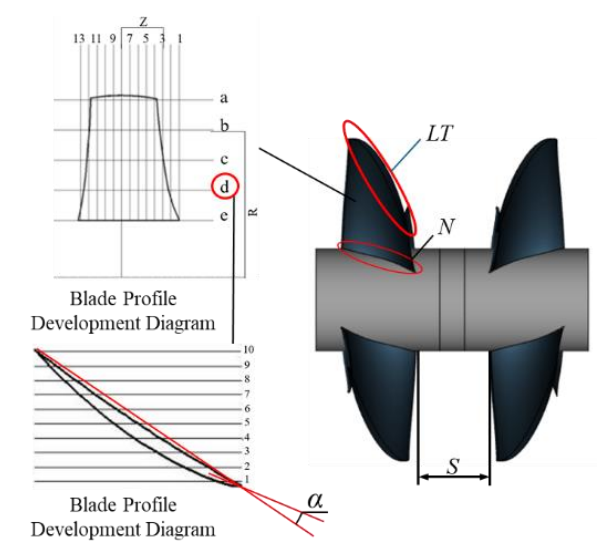


Fig. 2 Parameter modelling variables

geometric parameters governing impeller performance are specified in Table 1.

As shown in Fig. 2, the 4 parameterized variables of the reversible counter-rotating axial flow pump are marked in the figure.

#### 2.2 Numerical Simulation

#### 2.2.1 Numerical Schemes and Boundary Conditions

The controlling equations of fluid motion include the continuity equation, energy conservation equation, and momentum conservation equation. As the medium in the hydraulic machinery is incompressible water, generally, the energy conservation equation is not considered. Control equations by Reynolds time averaged processing become:

$$\frac{\partial \overline{v}_i}{\partial x_i} = 0 \tag{1}$$

$$\rho \left( \frac{\partial \overline{v}_i}{\partial t} + \overline{v}_j \frac{\partial \overline{v}_i}{\partial x_j} \right) = \rho f_i - \frac{\partial \overline{p}}{\partial x_i} + \frac{\partial}{\partial x_j} \left( \mu \frac{\partial \overline{v}_i}{\partial x_j} - \rho \overline{v}_i \overline{v}_j \right)$$
(2)

where  $\rho \overline{v_i'v_j'}$  is the Reynolds stress term due to turbulent motion,  $\bar{v}$  is the time-averaged velocity, m/s,  $\rho$  is the fluid density, kg/m<sup>3</sup>, and  $\mu$  is the dynamic viscosity, Pa·s.

In this study, ANSYS CFX – a finite volume method-based solver – is employed for numerical simulations, with the RNG k-ɛ turbulence model selected to resolve turbulent flow characteristics. This turbulence model represents an industry-standard approach that has been extensively validated for practical engineering applications, particularly in accurately capturing vortex formation under high strain rate conditions (Shao & Zhao, 2019).

For the forward operation mode of the pump, the rotational speed is initially set to 300 r/min, with the firststage and second-stage impellers rotating in opposite directions. The dynamic-static interface between rotating and stationary domains is treated using the frozen rotor method. The reference pressure is defined as 0 Pa, while the inlet boundary condition is specified as a pressure inlet with atmospheric pressure (101.325 kPa). The outlet boundary condition is configured as a mass flow outlet with a fixed value of 6000 kg/s. Wall boundaries adopt standard wall functions with no-slip conditions. The solution convergence criteria require all residual values to reach below 1×10<sup>-6</sup>. The convection term of the momentum equation is discretized using the upwind scheme, while the turbulent transport equations employ first-order spatial discretization. These numerical settings ensure solution stability while maintaining acceptable computational efficiency for the complex bidirectional flow simulations.

#### 2.2.2 Grid Division and Independence Verification

The computational domain is meshed using ANSYS ICEM with a multi-zone strategy. Refined grids are applied to the impeller blades and axial interstage gap to resolve complex flow features, while coarser grids are adopted for the inlet and outlet sections to optimize computational efficiency. To validate grid independence without compromising simulation accuracy or incurring excessive computational costs, a systematic grid convergence analysis is performed. The test results are presented in Fig. 3, where Eff denotes pump efficiency.

By observing Fig. 3, it can be found that when the grid count increases from 6.91 million to 8.08 million elements, the head and efficiency curves exhibit steep gradients with significant amplitude fluctuations. Beyond 8.08 million elements, these curves stabilize with minimal variation (<0.5%) under increasing grid density, indicating achieved mesh independence. Consequently, the optimal grid count is determined as 8.08 million elements. The meshing scheme uses a 23 mm element size for the impellers and interstage regions, and 30 mm for

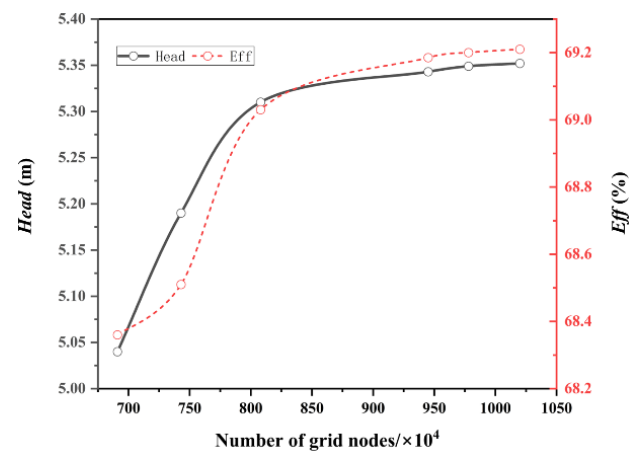


Fig. 3 Grid independence verification



Fig. 4 Grid diagram of reversible counter-rotating axial flow pump

other components. The final adopted mesh comprises 8.08 million elements, distributed with 3.22 million in the inlet section, 2.56 million in the outlet section, 1.02 million for the first-stage impeller, 1.02 million for the second-stage impeller, and 260,000 in the interstage region, as visualized in Fig. 4.

#### 2.3 Optimal Design Method

#### 2.3.1 Isight Platform Building

This study establishes an automated simulation workflow through the Isight integration platform, building upon the previously developed parametric modeling framework. As illustrated in Fig. 5, Isight orchestrates the sequential execution of all required numerical simulation tools through predefined process chains (Nyein et al., 2016).

After the post-flow field analysis, the hydraulic head and operational efficiency of the pump are systematically extracted as output metrics, subsequently mapped to predefined response variables within the Isight framework.

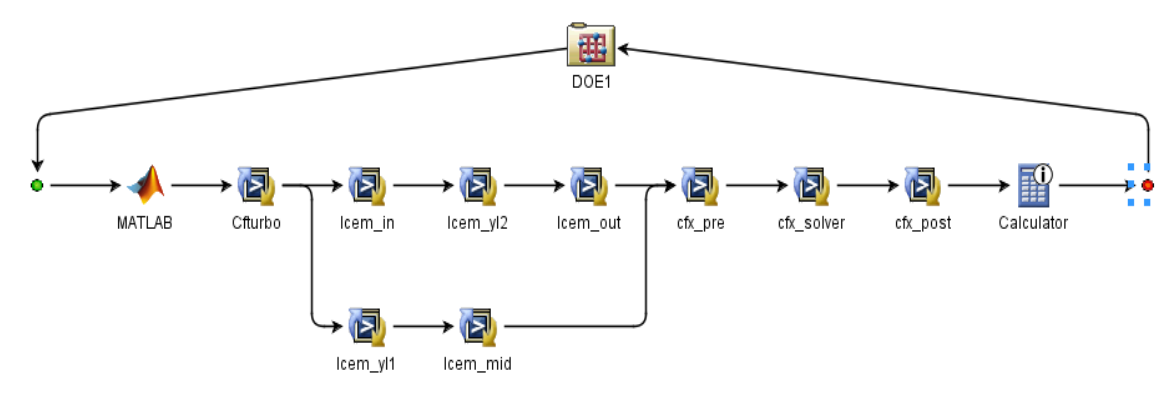


Fig. 5 Isight platform

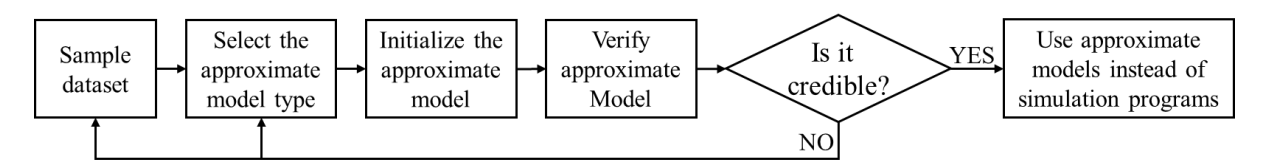


Fig. 6 Proxy model process

A Latin hypercube sampling (LHS) strategy (Cui et al., 2018) is implemented for input parameter optimization, ensuring design space uniformity and result reliability. This study employs 120 strategically distributed sample points (see Schedule A) to comprehensively characterize the parameter-performance relationship.

#### 2.3.2 Proxy Model

The experimental design yields 120 constrained parameter sets, which are utilized to construct surrogate models through response surface methodology (RSM) (Kim et al., 2021). These models establish continuous functional relationships between input factors and output responses (Bahrami & James, 2023), enabling the identification of optimal design configurations within the parameter space. The workflow for the surrogate modeling is shown in Fig. 6.

The surrogate modeling process utilizes the 120 experimental sample points obtained from the preceding design phase, with 90 datasets allocated for model construction and the remaining 30 reserved for error quantification. A comparative analysis of polynomial response surface models (second to fourth-order) is conducted for hydraulic head, efficiency, and shaft power parameters. Evaluation metrics revealed that second-order polynomial models demonstrated superior fitting accuracy with R² values of 0.99828 (head), 0.99491 (efficiency), and 0.99862 (shaft power), all exceeding the predetermined threshold of 0.9. Consequently, second-order response surface approximations are adopted for subsequent optimization iterations to balance numerical precision with operational efficiency.

#### 2.3.3 Multi-objective Optimal Design

At present, The Multi-Objective Genetic Algorithm (MOGA) implements the Pareto optimality criterion for fitness evaluation (May et al., 2015), and if a solution is

more improved than the previous generation in the sense of Pareto optimum, then it is considered that the fitness has been improved, and this is used as a criterion to evaluate the merit of an individual (Zolpakar et al., 2020). The Adaptive Mutation Genetic Algorithm (AMGA) improves the ability of global search by automatically adjusting the selection strategy (Zăvoianu et al., 2015; Sarro et al., 2017). To ensure the accuracy of the search, AMGA based on improved genetic algorithm is used in this paper. Among them, mutation coefficient and crossover probability are two very important parameters in genetic algorithm, which directly affect the search performance and convergence nature of the algorithm. The crossover operation combines the genes of two parents to create new individuals, thereby enhancing the population's diversity and search capability. Meanwhile, mutation helps maintain diversity and prevents the population from getting trapped in local optima by randomly modifying individual genes. To increase the algorithm's adaptability, the crossover probability and mutation rate are dynamically adjusted based on the state of the population.

The objective of this paper is to optimize a reversible axial flow pump with a head of not less than 5.3 m, minimizing the shaft power while maximizing the pump efficiency. We determined the approximate range of parameters by referring to the design process of a common axial flow pump. The specific objective function, constraints, and ranges of the design parameters are presented in Eqs. (3) - (5).

Objective function: 
$$\max Eff(x) \min P(x)$$
 (3)

Constrained conditions: 
$$H \ge 5.3$$
 (4)

Design variable: 
$$\begin{cases} 0 \le \alpha \le 4 \\ 0.67 \le LT \le 0.75 \\ 1.3 \le N \le 1.4 \\ 220 \le S \le 300 \end{cases}$$
 (5)

where:  $x = [\alpha, LT, N, S]^T$ .

#### 2.4 Experimental Methods

#### 2.4.1 Experimental Platform Construction

The experimental test rig, as depicted in Fig. 7, comprises the following key components: model pump unit, water tank, dual-gate valve system (Valve I & II), and interconnecting piping network. Critical measurement instrumentation includes an electromagnetic flowmeter, piezoresistive pressure transducers, a digital multimeter, and a tachometer.

Figure 7(a) illustrates the 3D-printed impeller mold with peripheral reinforcement rings to ensure dimensional fidelity during casting processes. The finalized impeller assembly, shown in Fig. 7(b), is manufactured through precision casting using cast iron. The pump's counterrotating impeller configuration employs a cantilevered mounting architecture on dual coaxial drive shafts, each independently powered by dedicated servo motors to enable bidirectional operation.

#### 2.4.2 Uncertainty Analysis

The multifunctional test bench integrates precision instrumentation with the following metrological specifications:

#### (1) Flowmeter

A KEFC-series electromagnetic flowmeter is installed upstream of the control valve to measure volumetric flow rate, and its measurement accuracy is 0.5%.

#### (2) Pressure transmitter

Differential pressure measurements are acquired using WT3000 transmitters (Wiltek Technologies) mounted on upstream and downstream pressure taps to measure hydraulic head. Its measurement accuracy is 0.2%.

#### (3) Digital Multimeter

Three-phase power parameters are monitored using a BK8E digital multimeter (Voltage: 100-400 V, Current: 1-5 A) with  $\pm 0.5\%$  reading accuracy.

#### (4) Tachometer

The DT2243C photoelectric tachometer is used to measure the rotational speed of each rotor shaft after the pump is running stably, and its accuracy is 0.05%. The overall measurement error is estimated from the measurement accuracy of each measurement unit described above.

$$e = \pm \sqrt[2]{0.5^2 + 3 \times 0.2^2 + 0.05^2 + 0.5^2} = \pm 0.79 \%$$
 (6)

The uncertainty of the test bench is  $\pm 0.79\%$ .

#### 3. RESULTS AND DISCUSSIONS

#### 3.1 Law of Influence of Parameters on Performance

Using the automatic optimization platform developed with Isight, the 120 sample points of design parameters in Schedule A are simulated, resulting in the heads and efficiencies of the pumps corresponding to various design parameter combinations, as shown in Schedule B.

Experimental evaluation of the 120 parametric configurations demonstrates hydraulic head variations between 3.46 m and 6.88 m, with corresponding efficiencies ranging from 67.7% to 72.8%. Sensitivity analysis reveals that design parameters exert more pronounced effects on head modulation compared to efficiency optimization. Figure 8 presents the iterative curves, which, based on optimized Latin hypercube sampling, confirm a uniform distribution within the design space and effectively illustrate the relationship between design parameters and pump performance.

To further understand the impact of design parameters and their interactions on the performance of the pump, a multiple quadratic regression model is established in Isight, as shown in Eq. (7).

$$Y = b_0 + \sum_{i=1}^{m} b_i x_i + \sum_{i=1}^{m} b_i x_i^2 + \sum_{i=1}^{i \neq j} b_{ij} x_i x_j$$
(7)

where  $b_0$ ,  $b_i$ , and  $b_{ij}$  denote the regression coefficients, and m denotes the number of factors. The regression model coefficients of the design parameters fitted by the test data with pump head and efficiency are shown in Table 2.

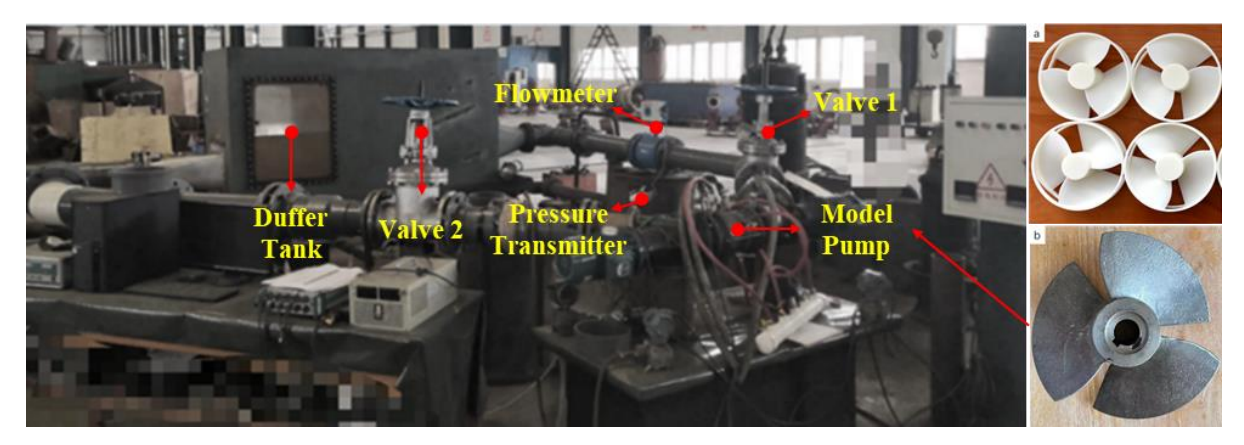


Fig. 7 Schematic of the experimental setup

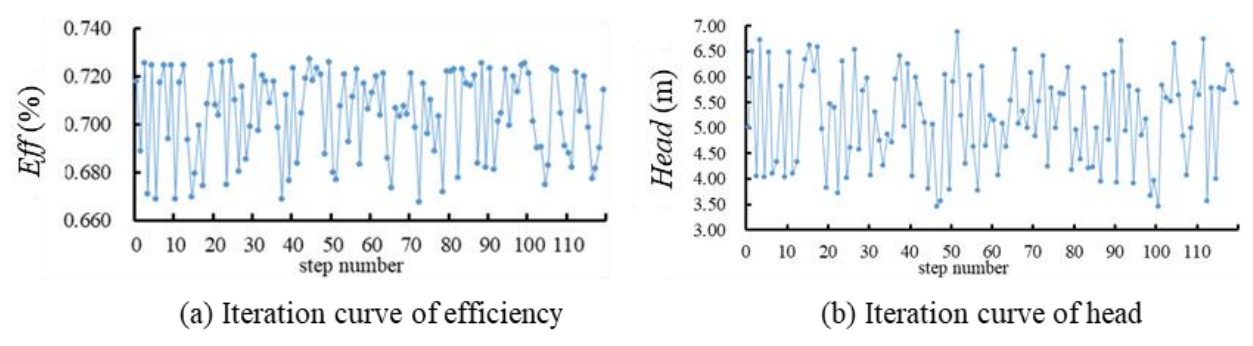


Fig. 8 Iteration curve chart

**Table 2 Regression model coefficients** 

$S_{i}$	α	LT	N	S	$\alpha^2$	$LT^2$	$N^2$	$S^2$	$\alpha$ -LT	α -N	α -S	LT-N	LT-S	N-S
Head	-0.04	4.13	-2.70	7.63	-0.06	-6.36	0.33	-36.24	0.56	0.20	0.93	0.91	20.03	5.81
Eff	-0.01	0.10	0.14	0.09		-0.06	-0.03	-0.51			0.01	-0.07	0.30	0.08

Table 3 ANOVA output results of head

	Head								
	DF	SS	V	F	*p*-value	R <sup>2</sup>			
Model	14.00	92.21	6.59	8544.10	< 0.001	0.99			
Error	96.00	0.07	/	/	/	/			
Total	110.00	92.29	/	/	/	/			

Table 4 ANOVA output results of efficiency

	Eff								
	DF	SS	V	F	*p*-value	R <sup>2</sup>			
Model	14.00	0.03	0.02	2430.05	< 0.001	0.99			
Error	96.00	0.01	/	/	/	/			
Total	110.00	0.04	/	/	/	/			

As shown in the table, the hydraulic performance of axial flow pumps is influenced not only by the linear terms of the design parameters but also by second-order main effects and the interaction effects among different design parameters. To test the significance of the regression equation, this paper employs analysis of variance (ANOVA). The results of the ANOVA are presented in Tables 3 and 4 (Liao et al. 2020; Betchem et al. 2023).

As shown in Tables 3 and 4, DF represents the degree of freedom, SS denotes the sum of squared deviations from the mean, V is the mean square, and R<sup>2</sup> indicates the fitting accuracy. The closer R<sup>2</sup> is to 1, the higher the fitting accuracy. ANOVA directly reveals whether the main and interaction effects of the design parameters are significant.

## 3.1.1 Study of the Main Effect of Design Parameters on Pump Performance

The main effect of a factor pair response is the average response of the factor across all trials at a specific level. This averages the effects on the results by varying the level of a single factor while considering all possible combinations of each level and the other factors. The main

effects of the design parameters of the reversible counterrotating axial flow pump on pump performance are shown in Fig. 9.

As illustrated in the figure, the attack angle exhibits a linear and positive correlation with head in the first half and a nonlinear positive correlation in the second half. The vane placement angle increases with the attack angle, resulting in enhanced pump work capacity. The relationship between axial interstage gap and head is nonlinear, they are positively correlated in the first half and negatively correlated in the second half, indicating the existence of an optimal threshold value. When this threshold is exceeded, losses along the stroke between the two-stage impeller increase, leading to a reduction in the pump's power generation capacity. The *L* and *N* are linearly and positively correlated with head.

In terms of efficiency, the main effect of the attack angle is negatively correlated with the head. As the attack angle increases, it can lead to flow separation, reducing efficiency. In reversible axial flow pumps, the first impeller's inlet precession requires an increased attack angle to maintain flow. However, since the reversible counter-rotating axial flow pumps analyzed in this paper

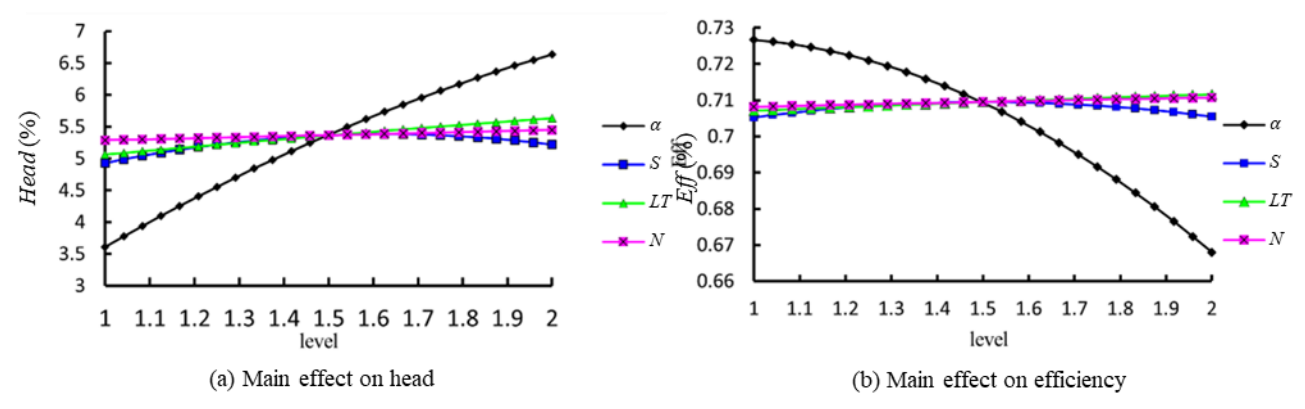


Fig. 9 Main effect diagram

maintain the same impeller blade placement angle in both stages to accommodate both forward and reverse operating conditions, an increased attack angle in the second-stage impeller may decrease efficiency. Therefore, selecting an appropriate attack angle is essential to balance both head and efficiency. The main effect of the LT and N on efficiency is positive but not significant. Similarly, the effect of axial interstage gap on efficiency mirrors that of the head, with an initial positive correlation in the first half followed by a negative correlation in the second half after a certain cutoff point.

#### 3.1.2 Design Parameter Interaction Effects Analysis

The interaction effect represents the interdependence and mutual constraints among two or more factors, which together influence changes in the response variable. The interaction effect plot, derived from the main effect analysis, illustrates how two factors jointly affect the response. It depicts the relationship and strength of the interaction by showing the main effect of the first factor at different levels of the second factor. In the experimental design, there are four design variables, which ultimately constitute 12 interaction pairs affecting the two response variables. The interaction effects of the design parameters on head and efficiency are presented in Figs. 10 and 11, respectively.

For the head, Fig. 10 shows that the interaction effect between the attack angle and the axial interstage gap is the most significant, as indicated by the crossing curves. In contrast, the interaction effects between N and axial interstage gap, as well as between LT and axial interstage gap, are negligible. The interaction effect curves for the attack angle and N, and for LT and N, are parallel, indicating no interaction. Together with the main effect analysis, these results suggest that the attack angle has the most significant main effect on the head, while the axial interstage gap exhibits a threshold effect, confirming the reliability of the main effect conclusions. The interaction between attack angle and axial interstage gap mainly reflects the working capacity of the second-stage impeller. Moreover, the axial interstage gap length influences the inlet precession of the second-stage impeller, implying an optimal parameter range for these two factors.

For efficiency, Fig. 11 illustrates that the interaction effects are essentially the same as those observed for head. The most significant interaction occurs between the attack angle and the axial interstage gap, while the interactions

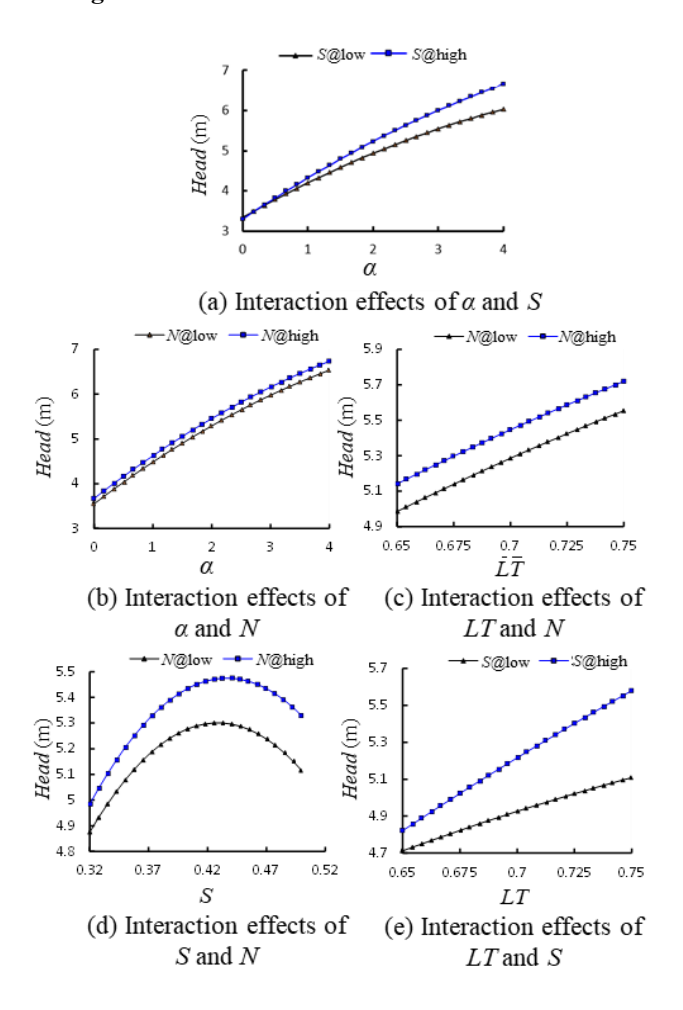


Fig. 10 Graph of the interaction effect of design parameters on head

between the axial interstage gap and LT, as well as the N, are insignificant. No interaction effects are observed among the other parameters. Combined with the main effect analysis, the attack angle remains the most influential factor, indicating an optimal relationship between the axial interstage gap and the attack angle. Notably, changes in the attack angle affect the blade inlet flow angle, which subsequently alters the flow path and velocity distribution within the impeller. It can induce localized flow separation and vortex formation, influencing the leakage flow in the interstage gap. The characteristics of this leakage flow significantly impact pump efficiency, as changes in the attack angle modify the

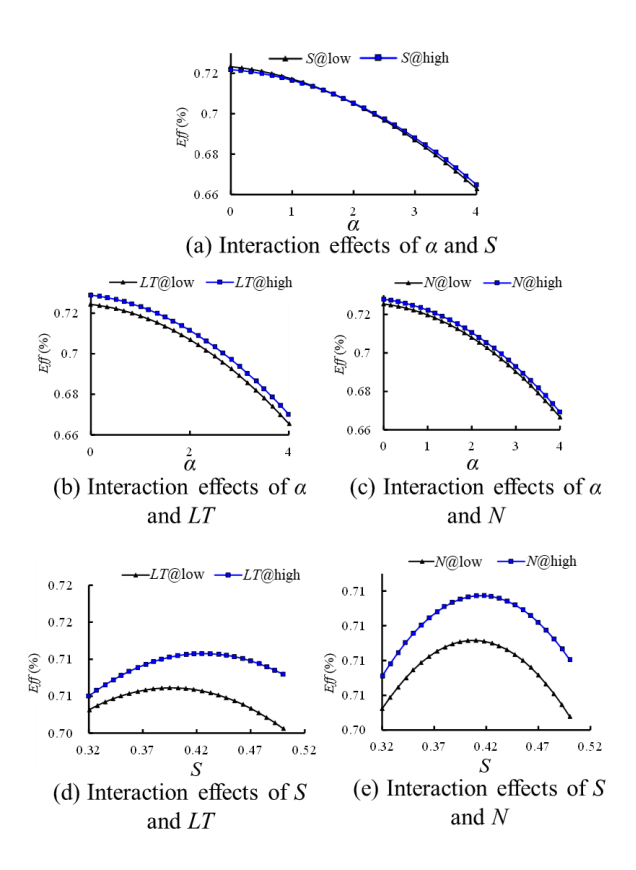


Fig. 11 Graph of the interaction effect of design parameters on efficiency

pressure gradient and rotational behavior of the leakage flow. The combined effect of these factors can either enhance or suppress vortex structures, leading to nonlinear energy losses and fluctuations in performance.

### 3.1.3 Analysis of the Contribution Rate of Design Parameters

By fitting the input variables using least squares after normalizing them to the range of [-1, 1], a new set of

model coefficients is obtained, which more accurately reflects the contribution of each input variable to the response. These values are presented in Table 5. To clarify the percentage contribution of each factor, the normalized model coefficients are transformed according to Eq. (8).

$$N_{X_i} = \frac{100S_{x_i}}{\sum_{j} |S_{x_i}|} \tag{8}$$

After removing the factors with low contribution rates, the adjusted contribution rates are shown in Fig. 12, sorted by the absolute value of their percentage contributions. Blue indicates a positive effect, while red indicates a negative effect. Pump performance is influenced not only by the linear effects of individual factors but also by their second-order terms and interaction effects.

For the head, the linear contribution of the attack angle is the largest at 51.28%, consistent with the main effect analysis. The contributions of the other individual factors rank as follows: LT > S > N, each contributing less than 10%, with N accounting for only 2.74%. Notably, the interaction effect between the attack angle and the axial interstage gap contributes 5.66%, exceeding the linear contributions of both the axial interstage gap and the N. It highlights the significant influence of these two factors on the head, in agreement with the interaction effect analysis. For efficiency, the linear contribution of the attack angle reaches a maximum of 56.2%, but it has a negative effect. The same design parameters significantly influence both the head and efficiency of the pump, though in opposite directions. The contribution rates of the other individual factors are ranked as follows: LT > N > S, with the axial interstage gap contributing the least at only 0.24%. Regarding interaction effects, the combined contribution of LT and axial interstage gap to efficiency is 2.62%, compared to 3% for head. It highlights that LT is an important design parameter, affecting performance both individually and through interactions with other factors.

Table 5 Ta	able of	normalized	coefficients
------------	---------	------------	--------------

$S_i$	α	LT	N	S	$\alpha^2$	$LT^2$	$N^2$	$S^2$	α-LT	$\alpha$ -N	α -S	LT-N	LT-S	N-S
Head	1.51	0.29	0.08	0.15	-0.25	-0.02	/	-0.29	0.06	0.02	0.17	/	0.09	0.03
Eff	-0.01	/	/	/	-0.01	/	/	/	/	/	/	/	/	/

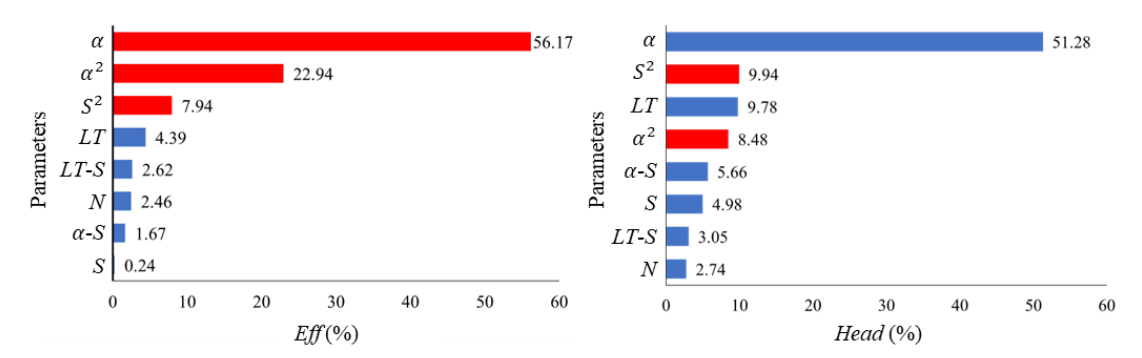


Fig. 12 Contribution of design parameters

α	LT	N	S	Eff	Head	P
		1504	iterations of calcu	ılation		
1.72516	0.73171	1.34360	312.40053	0.71470	5.32252	438.14742
1.70659	0.73851	1.31215	315.67677	0.71438	5.30042	436.46567
1.69857	0.73171	1.39222	291.97781	0.71614	5.33395	438.20873
1.60987	0.73863	1.39863	314.72672	0.71799	5.35380	438.93105
		900	4 iterations calcu	lated		
1.46865	0.74996	1.40000	316.26414	0.72028	5.30002	433.21824
1.46865	0.74996	1.40000	316.26414	0.72028	5.30002	433.21824
1.46865	0.75000	1.40000	316.26498	0.72028	5.30026	433.23758
1.46865	0.74999	1.40000	316.14848	0.72028	5.30005	433.21930
		15004	iterations of calc	ulation		
1.46577	0.75000	1.40000	318.27298	0.72031	5.30000	433.21091
1.46464	0.75000	1.40000	319.26212	0.72032	5.30000	433.21157
1.46464	0.75000	1.40000	319.26642	0.72032	5.30003	433.21373
1.46464	0.75000	1.40000	319.26642	0.72032	5.30003	433.21377
1.46464	0.75000	1.40000	319.26212	0.72032	5.30002	433.21273

**Table 6 Objective function Pareto solution set** 

Table 7 Comparison of parameters before and after optimization

	α	LT	N	S	Eff	Head	P
Initial value	2.40	0.67	1.30	386.00	0.69	5.31	447.70
Optimization value	1.46	0.75	1.40	319.26	0.72	5.30	433.21

#### 3.2 Multi-objective Optimization Analysis

The final Pareto solution sets for the objective functions under constrained conditions are obtained using the Adaptive Multi-Objective Genetic Algorithm (AMGA) after 1,504, 9,004, and 15,004 iterations for head, efficiency, and shaft power, respectively, as shown in Table 6.

According to Table 6, the AMGA optimization identifies the pump design parameters and performance indicators at their optimal values within the design space. The results before and after optimization are summarized in Table 7, showing a 3% increase in efficiency and a reduction in shaft power by 14.5 kW, while maintaining the same head. After optimization, the vane attack angle decreases, while LT and N reach their maximum constraint limits, resulting in increased cascade density and impeller blade area, along with reduced differential pressure and relative velocity. For axial pumps, hydraulic losses are proportional to the geometric mean of the relative velocities. Therefore, minimizing this geometric mean reduces losses. The optimized axial interstage gap values are moderate rather than extreme, suggesting that very small or very large clearances are suboptimal.

The hydraulic performance of the reversible counterrotating axial flow pump is predicted through numerical simulation both before and after optimization. The pump head efficiency and shaft power are calculated using Eqs. (9)  $\sim$  (11), respectively, to derive the flow-head and flowefficiency curves shown in Fig. 13. Here, *Head-*1 and *Eff*-1 represent the head and efficiency of the optimized pump, while *Head-*0 and *Eff-*0 denote the head and efficiency of the initial pump.

$$H = \frac{P_{out} - P_{in}}{\rho g} \tag{9}$$

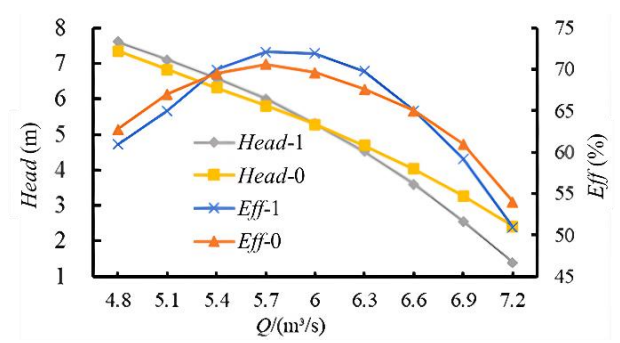


Fig. 13 External characteristic curve before and after optimization

$$Eff = \frac{\rho gQH}{P} \tag{10}$$

$$P = \frac{2\pi nT}{60} \tag{11}$$

where:  $P_{out}$  - pump outlet pressure, Pa.  $P_{in}$  - pump inlet pressure, Pa. T- Torque, N·m.

From the figure, it can be seen that the difference in head between the optimized and initial pumps is negligible before reaching the design flow condition. However, beyond this point, the head of the optimized model declines more rapidly than that of the initial model (Shi et al. 2020). This behavior is attributed to the reduced attack angle after optimization. Under high flow conditions, the smaller attack angle leads to insufficient pre-rotation at the vane inlet, thereby reducing work capacity of the pump. The efficiency curve shows that the optimal operating points of both pumps shift toward lower flow rates after optimization. Near the design operating point, the

optimized pump achieves significantly higher efficiency than the initial model.

#### 3.3 Internal Flow Analysis

Figs. 14 and 15 present velocity distribution contour plots at different radial coefficients and at the inlet of the second-stage impeller before and after optimization under the design flow condition. Figs. 16 and 17, meanwhile, show their pressure distribution contour plots. To support the following analysis, the span normalization (*sn*) is defined as follows:

$$sn = \frac{R - r_h}{R_D - r_h} \tag{12}$$

where: R-radius of the calculated section, mm,  $R_D$ -radius at the wheel rim, mm,  $r_h$ - radius at the wheel hub, mm.

#### 3.3.1 Variation of Velocity

Figure 14 demonstrates that the high-velocity region A on the optimized blade suction surface substantially exceeds region B of the initial model at sn=0.2, confirming enhanced energy transfer capability near the impeller hub post-optimization. Both pre- and post-optimization configurations exhibit concentrated high-

velocity zones at the second-stage impeller leading edge (sn = 0.2), and progressively expanding across the entire suction surface as sn increases. This distribution stems from greater airfoil curvature and thickness near the hub versus gradual profile transitions at the rim, promoting velocity uniformity. Crucially, the high-velocity region development on the second-stage suction surface influences the first-stage pressure surface, an effect most pronounced in the initial model that impairs energy conversion efficiency. Post-optimization, increased hub and rim cascade densities (indicative of extended chord length) yield more uniform blade surface velocity and pressure distributions, thereby mitigating adverse interstage interactions.

To analyze the effect of the axial interstage gap on pump performance, Figs. 15 and 18 show the velocity and pressure distributions at the inlet of the second-stage impeller before and after optimization. Since the impeller has three blades, Fig. 15 displays three high-pressure and three low-pressure zones distributed in phase. After optimization, in regions C and D, the gap between the two impellers is reduced, theoretically increasing the interference between them and making the periodicity of the velocity distribution more pronounced.

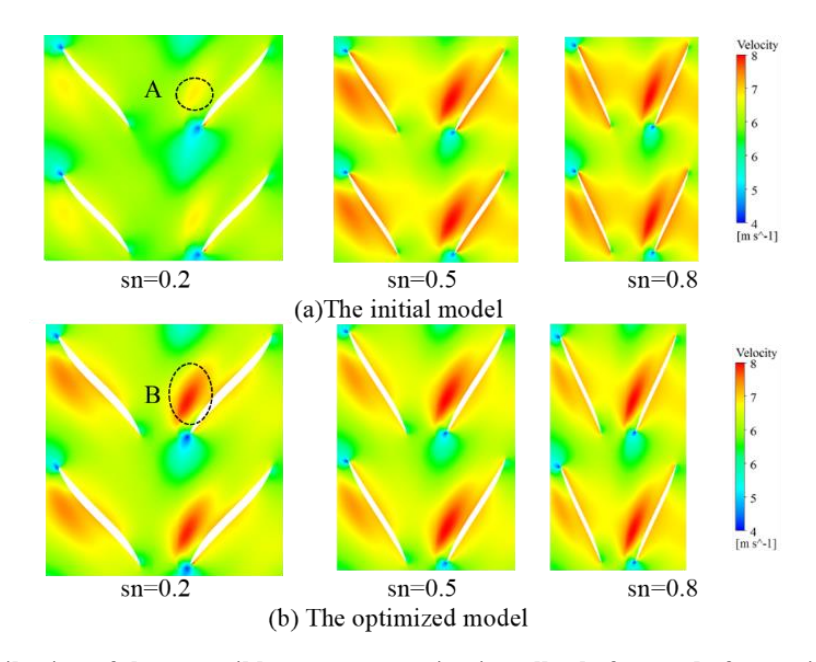


Fig. 14 Velocity distribution of the reversible counter-rotating impeller before and after optimization at different radial coefficients

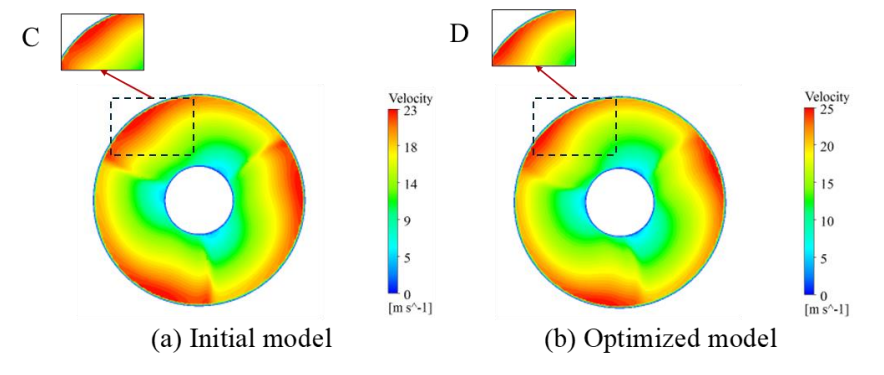


Fig. 15 Second-stage impeller inlet velocity distribution

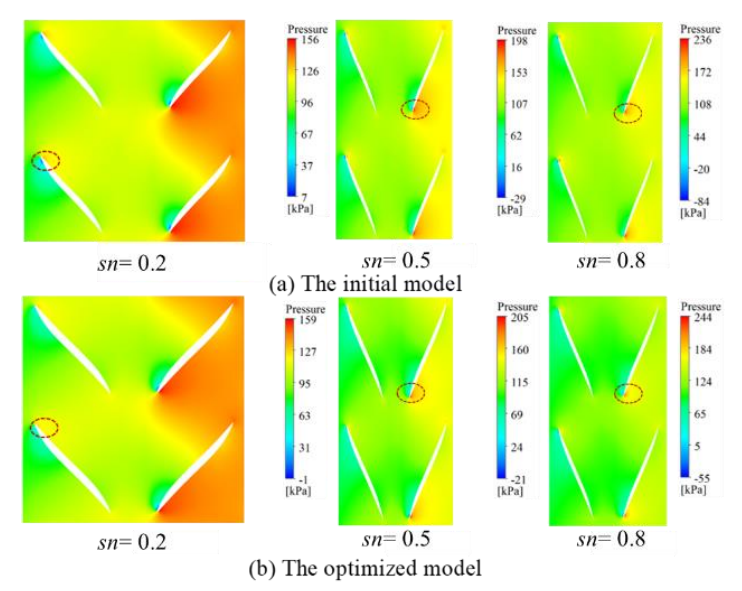


Fig. 16 Pressure distribution of the reversible counter-rotating impeller before and after optimization at different radial coefficients

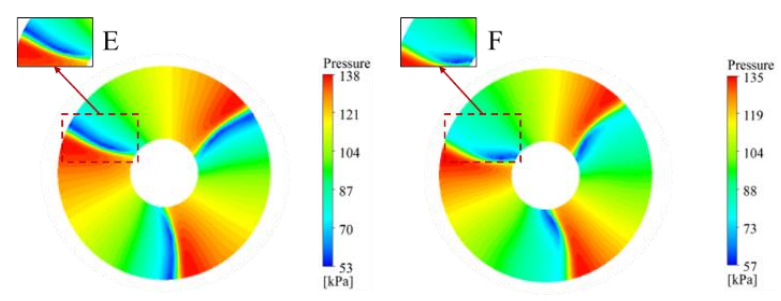


Fig. 17 Second-stage impeller inlet pressure distribution

#### 3.3.2 Variation of Pressure

As observed in Fig. 16, the initial model's excessive attack angle concentrates pressure differentials near the leading edge (sn = 0.2-0.8). It accelerates flow separation at the trailing edge due to impeller inflow impact and blade edge geometry, degrading efficiency. Optimization reduces attack angles for both impellers, distributing pressure uniformly from the leading to the trailing edges. This modification improves flow transition from the first-stage outlet to the second-stage inlet, particularly critical in counter-rotating designs where firststage outflow directly governs second-stage energy transfer capacity. Consequently, attack angle reduction significantly enhances overall pump efficiency.

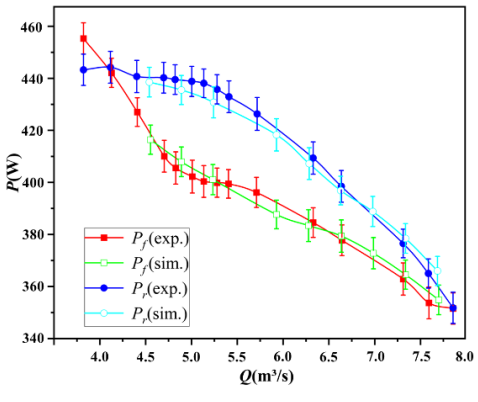
As illustrated in Fig. 15 and Fig. 17, the pressure distribution characteristics at the inlet section of the second-stage impeller before and after optimization closely resemble the velocity distribution. In the pressure cloud depicted in Fig. 17, the initial model exhibits a low-pressure zone E near the blade head that extends from the hub to the rim. In contrast, the optimized model features a low-pressure region F that does not extend near the rim. This difference arises because, in the optimized design, the rim side of the second-stage impeller blade is positioned further away from the intersection surface when the fluid from the first-stage impeller has not yet reached the blade head, preventing the formation of a low-pressure area.

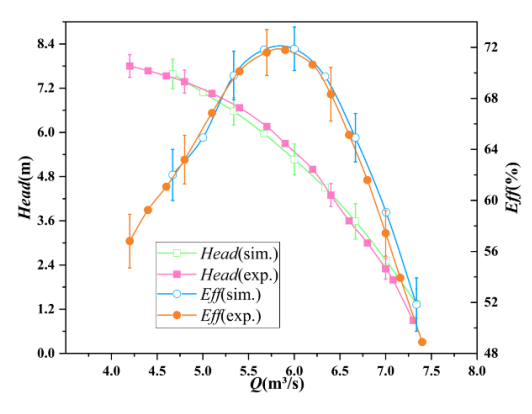
#### 3.3.3 Experimental Verification

Figure 18 compares experimentally measured and numerically simulated pump performance characteristics. In Fig. 19(a), test-derived head and efficiency curves demonstrate close alignment. While the numerical simulation results in slightly higher efficiency values than the test results for flow rates above 100 m³/h, the discrepancy remains within 2%. Between 50-80 m³/h, head calculations exhibit a maximum 4% deviation. Confidence intervals confirm measurement reliability, with head at 5.3 m [4.84, 5.76] and efficiency at 72% [69.58, 74.18].

Figure 18(b) depicts flow rate versus shaft power (Q -  $P_e$ ), where  $P_f$  and  $P_r$  denote first and second-stage impeller shaft power, respectively. Both experimentally and numerically derived Q -  $P_e$  curves show smooth monotonic reduction. Although stage-specific power magnitudes differ across operating conditions, both stages maintain consistent power reduction trends throughout the flow range, with experimental and numerical results exhibiting strong agreement.

Significant rotor-rotor interactions and complex internal flows in reversible counter-rotating impellers increase flow field instability. This complexity contributes to steady-state numerical head prediction errors. Full-flow conditions demonstrate excellent experimental-numerical





(a) Total head and efficiency

(b) Shaft power of two-stage impeller

Fig. 18 Test verification

consistency, confirming the simulation's reliability for design optimization.

4. CONCLUSIONS

This paper uses the DOE to analyze how the main design parameters of a reversible counter-rotating axial flow pump influence its hydraulic performance. It shows both the primary and secondary relationships among these parameters and their effects on performance. Utilizing the Isight platform, we developed an optimization process to simulate scenarios derived from the experimental design. A response surface model is established to correlate the main design parameters with pump performance. Finally, a multi-objective optimization algorithm is employed for a global search of the optimal combination of the mathematical model, leading to the best design parameter set, which is validated through numerical simulations and tests. The key findings are as follows:

- (1) For head and efficiency, the main and interaction effects are nearly identical. Notably, the attack angle has the most significant impact on both head and efficiency, with contribution rates of 51.28% and 56.2%, respectively; however, efficiency exhibits a negative contribution rate. Among all parameters, the interaction effects between the axial interstage gap and attack angle are most pronounced.
- (2) It shows that the density increases at the hub and rim of the impeller at different radial coefficients. The velocity and pressure variations are more uniform on the blade surface, and the influence of the high-speed zone of the second-stage impeller on the first-stage impeller is mitigated.
- (3) It indicates that reducing the attack angle of the first-stage impeller leads to a more uniform pressure distribution across the blade surface from head to tail. The adjustment enhances flow conditions in the second-stage impeller, increasing the operational efficiency of the pump.
- (4) The simulation efficiency of the optimized reversible counter-rotating axial flow pump at the design operating point is 3% higher than pre-optimization, with a reduction in shaft power by 14.5 kW. Experimental results

further validate the consistency between numerical simulations and practical outcomes.

#### **ACKNOWLEDGMENTS**

This work is funded by the National Natural Science Foundation of China [52409116], Shandong Province science and technology SMES innovation ability improvement project [2023TSGC0005].

#### **COMPETING INTERESTS**

The authors declare that they have no competing interests.

#### **AUTHORS CONTRIBUTIONS:**

Qingjiang Xiang: Writing-original draft, Conceptualization. Delong Kong: Writing-original draft, Writing-review & editing. Wei Xu: Software, Data curation. Xiuli Wang: Software, Visualization. Yajie Xie: Data curation, Validation. Yuanyuan Zhao: Resources, Supervision, Funding acquisition.

#### REFERENCES

An, C., Chen, Y., Fu, Q., & Zhu, R. (2023). Internal Flow Phenomena of Two-Way Contra-Rotating Axial flow Pump-Turbine with Various Numbers of Blades in Pump Mode. *Water*, *15*(18), 3236. https://doi.org/10.47176/jafm.16.02.1140

Bahrami, P., & James, L. A. (2023). Screening of waterflooding using smart proxy model coupled with deep convolutional neural network. *Geoenergy Science and Engineering*, 221, 111300. https://doi.org/10.1016/j.petrol.2022.111300

Betchem, G., Dabbour, M., Tuly, J. A., Billong, L. F., & Ma, H. (2023). Optimization of fermentation conditions to improve the functional and structural characteristics of rapeseed meal with a mutant Bacillus subtilis species. *Industrial Crops and Products*, 205, 117424. https://doi.org/10.1016/j.indcrop.2023.117424

Chen, Y., An, C., Zhang, R., Fu, Q., & Zhu, R. (2023).

- Research on two-way contra-rotating axial flow pump~turbine with various blade angles in pump mode. *Processes*, 11(5), 1552.
- Cui, L., Mao, H., Xue, X., Ding, S., & Qiao, B. (2018). Optimized design and test for a pendulum suspension of the crop spray boom in dynamic conditions based on a six DOF motion simulator. *International Journal of Agricultural and Biological Engineering*, 11(3), 76-85. https://doi.org/10.25165/j.ijabe.20181103.3717
- Fahlbeck, J., Nilsson, H., Salehi, S., Zangeneh, M., & Joseph, M. (2021, June). Numerical analysis of an initial design of a counter-rotating pump-turbine. *In IOP Conference Series: Earth and Environmental Science* (Vol. 774, No. 1, p. 012066). IOP Publishing. <a href="https://doi.org/10.1088/1755-1315/774/1/012066">https://doi.org/10.1088/1755-1315/774/1/012066</a>
- Gao, X., Tian, Y., & Sun, B. (2018). Multi-objective optimization design of bidirectional flow passage components using RSM and NSGA II: A case study of inlet/outlet diffusion segment in pumped storage power station. *Renewable Energy*, 115, 999-1013.
- Harris, P, Wolf, T, Kesseli, J, & Laughlin, R. B. (2020). An Investigation of Reversing Axial Turbomachinery for Thermal Energy Storage Application." Proceedings of the ASME Turbo Expo 2020: Turbomachinery Technical Conference and Exposition. Volume 5: Controls, Diagnostics, and *Instrumentation;* Cycle *Innovations;* Cycle Innovations: Energy Storage. Virtual, Online. September 21-25, 2020. V005T07A003. ASME. https://doi.org/10.1115/GT2020-15286
- Hoffstaedt, J. P., Truijen, D. P. K., Fahlbeck, J., Gans, L. H. A., Qudaih, M., Laguna, A. J., De Kooning, J.D.M., Stockman, K., Nilsson, H., Storli, P.-T., Engel, B., Marence, M. & Bricker, J. D. (2022). Lowhead pumped hydro storage: A review of applicable technologies for design, grid integration, control and modelling. *Renewable and Sustainable Energy Reviews*, 158, 112119. https://doi.org/10.1016/j.rser.2022.112119
- Hu, Z., Cheng, Y., Liu, D., Chen, H., Ji, B., & Ding, J. (2023). Broadening the operating range of pumpturbine to deep-part load by runner optimization. Renewable Energy, 207, 73-88. https://doi.org/10.1016/j.renene.2023.03.005
- Huang, J., Tan, L., Tian, K., Zhang, B., Ji, A., Liu, H., & Shen, C. (2023). Formation mechanism for the laying angle of hemp harvester based on ANSYS-ADAMS. *International Journal of Agricultural and Biological Engineering*, 16(4), 109-115. https://doi.org/10.25165/j.ijabe.20231604.7978
- Kan, K., Zhang, Q., Xu, Z., Chen, H., Zheng, Y., Zhou, D., & Binama, M. (2021). Study on a horizontal axial flow pump during runaway process with bidirectional operating conditions. *Scientific Reports*, 11(1), 1-21. <a href="https://doi.org/10.1038/s41598-021-01250-1">https://doi.org/10.1038/s41598-021-01250-1</a>
- Kim, J. W., Suh, J. W., Choi, Y. S., Lee, K. Y., Kanemoto, T., & Kim, J. H. (2018). Optimized Blade Design of

- Counter-Rotating-Type Pump-Turbine Unit Operating in Pump and Turbine Modes. *International Journal of Rotating Machinery*, 2018(1), 6069780.
- Kim, J. W., Suh, J. W., Choi, Y. S., Lee, K. Y., Kim, J. H., Kanemoto, T., & Kim, J. H. (2016). Simultaneous efficiency improvement of pump and turbine modes for a counter-rotating type pump-turbine. *Advances in Mechanical Engineering*, 8(11), 1687814016676680. https://doi.org/10.1177/1687814016676680
- Kim, J., Lee, K., & Choe, J. (2021). Efficient and robust optimization for well patterns using a PSO algorithm with a CNN-based proxy model. *Journal of Petroleum Science and Engineering*, 207, 109088. <a href="https://doi.org/10.1016/j.petrol.2021.109088">https://doi.org/10.1016/j.petrol.2021.109088</a>
- Liao, J., Luo, X., Wang, P., Zhou, Z., O'Donnell, C. C., Zang, Y., & Hewitt, A. J. (2020). Analysis of the influence of different parameters on droplet characteristics and droplet size classification categories for air induction nozzle. *Agronomy*, *10*(2), 256. https://doi.org/10.3390/agronomy10020256
- Ma, P., & Wang, J. (2017). An analysis on the flow characteristics of bi-directional axial flow pump under reverse operation. Proceedings of the Institution of Mechanical Engineers, Part A: *Journal of Power and Energy*, 231(3), 239-249. https://doi.org/=10.1177/0957650917695447
- Mansour, M., Zähringer, K., Nigam, K. D., Thévenin, D., & Janiga, G. (2020). Multi-objective optimization of liquid-liquid mixing in helical pipes using Genetic Algorithms coupled with Computational Fluid Dynamics. *Chemical Engineering Journal*, 391, 123570. https://doi.org/10.1016/j.cej.2019.123570
- May, G., Stahl, B., Taisch, M., & Prabhu, V. (2015). Multi-objective genetic algorithm for energy-efficient job shop scheduling. *International Journal of Production Research*, 53(23), 7071-7089. <a href="https://doi.org/10.1080/00207543.2015.1005248">https://doi.org/10.1080/00207543.2015.1005248</a>
- Nyein, S. M., Xu, H., & Yu, H. (2016). Parametric Optimization of Vortex Shedder based on Combination of Gambit, Fluent and iSIGHT. *International Journal of Fluid Machinery and Systems*, 9(2), 150-158. https://doi.org/10.5293/IJFMS.2016.9.2.150
- Qin, Y., Li, D., Wang, H., Liu, Z., Wei, X., & Wang, X. (2022). Multi-objective optimization design on high pressure side of a pump-turbine runner with high efficiency. *Renewable Energy*, 190, 103-120. https://doi.org/10.1016/j.renene.2022.03.085
- Sarro, F., Ferrucci, F., Harman, M., Manna, A., & Ren, J. (2017). Adaptive multi-objective evolutionary algorithms for overtime planning in software projects. *IEEE Transactions on Software Engineering*, 43(10), 898-917. <a href="https://doi.org/10.1109/TSE.2017.2650914">https://doi.org/10.1109/TSE.2017.2650914</a>
- Shao, X., & Zhao, W. (2019). Performance study on a partial emission cryogenic circulation pump with high head and small flow in various conditions.

International Journal of Hydrogen Energy, 44(49), 27141-27150.

https://doi.org/10.1016/j.ijhydene.2019.08.181

- Sharma, S., & Kumar, V. (2022). A comprehensive review on multi-objective optimization techniques: Past, present and future. *Archives of Computational Methods in Engineering*, 29(7), 5605-5633. https://doi.org/10.1007/s11831-022-09778-9
- Shi, L., Tang, F., Zhou, H., Tu, L., & Xie, R. (2015). Axial flow pump hydraulic analysis and experiment under different swept-angles of guide vane. *Transactions of the Chinese Society of Agricultural Engineering*, 31(14), 90-95.
- Shi, L., Zhang, W., Jiao, H., Tang, F., Wang, L., Sun, D., & Shi, W. (2020). Numerical simulation and experimental study on the comparison of the hydraulic characteristics of an axial flow pump and a full tubular pump. *Renewable Energy*, 153, 1455-1464. https://doi.org/10.1016/j.renene.2020.02.082
- Vashahi, F., Lee, S., & Lee, J. (2017). Experimental and computational analysis of the swirling flow generated by an axial counter-rotating swirler in a rectangular model chamber using water test rig. *Journal of Engineering for Gas Turbines and Power*, *139*(8). https://doi.org/10.1115/1.4035734
- Wang, C., Zhang, Y., Liu, Z., & Yuan, Z. (2022). Multiobjective optimization of a two-stage liquefied natural gas cryogenic submerged pump-turbine in pump mode to reduce flow loss and cavitation. *Journal of Energy Storage*, 52, 105064. https://doi.org/10.1016/j.est.2022.105064
- Xie, C., Feng, A., Fu, T., Zhang, C., Zhang, T., & Yang, F. (2022). Analysis of Energy Characteristics and Internal Flow Field of 'S' Shaped Airfoil Bidirectional Axial Flow Pump. *Water*, *14*(18), 2839.

### Xiuli, W., Bin, L., Yang, L., Yan, Z., Rongsheng, Z., Yun, L., & Qiang, F. (2020). Hydraulic optimization of two-way counter-rotating axial flow pump turbine. Frontiers in Energy Research, 8, 577232. https://doi.org/10.3389/fenrg.2020.577232

- Xu, F., Wang, B., Hong, C., Telebielaigen, S., Nsor-Atindana, J., Duan, Y., & Zhong, F. (2019).
   Optimization of spiral continuous flow-through pulse light sterilization for Escherichia coli in red grape juice by response surface methodology. *Food Control*, 105, 8-12.
   <a href="https://doi.org/10.1016/j.foodcont.2019.04.023">https://doi.org/10.1016/j.foodcont.2019.04.023</a>
- Zăvoianu, A. C., Lughofer, E., Bramerdorfer, G., Amrhein, W., & Klement, E. P. (2015). DECMO2: a robust hybrid and adaptive multi-objective evolutionary algorithm. *Soft Computing*, *19*, 3551-3569. https://doi.org/10.1007/s00500-014-1308-7
- Zhang, W., Tang, F., Shi, L., Hu, Q., & Zhou, Y. (2020a). Effects of an inlet vortex on the performance of an axial flow pump. *Energies*, 13(11), 2854. <a href="https://doi.org/10.3390/en13112854">https://doi.org/10.3390/en13112854</a>
- Zhang, D., Katayama, Y., Watanabe, S., Tsuda, S. I., & Furukawa, A. (2020b). Performance prediction model of contra-rotating axial flow pump with separate rotational speed of front and rear rotors and its application for energy saving operation. *Journal of Fluid Science and Technology*, *15*(3), JFST0015-JFST0015. <a href="https://doi.org/10.1299/jfst.2020jfst0015">https://doi.org/10.1299/jfst.2020jfst0015</a>
- Zolpakar, N. A., Lodhi, S. S., Pathak, S., & Sharma, M. A. (2020). Application of multi-objective genetic algorithm (MOGA) optimization in machining processes. *Optimization of Manufacturing Processes*, 185-199. <a href="https://doi.org/10.1007/978-3-030-19638-7.8">https://doi.org/10.1007/978-3-030-19638-7.8</a>

#### **APPENDIX**

## Schedule A Optimal Latin Hypercube Design Matrix

Sample Points	α <sub>/(°)</sub>	S/(mm)	LT	N
1	1.513	282	0.71387	1.33866
2	3.16	374.3	0.72899	1.39748
3	0.605	310.8	0.66849	1.38403
4	3.899	377.3	0.70294	1.37311
5	0.37	372.8	0.73487	1.34958
6	3.933	344	0.67689	1.3437
7	0.84	389.4	0.67857	1.31345
8	0.706	328.9	0.71891	1.33193
9	2.756	368.2	0.68445	1.3605
10	0.37	372.8	0.73487	1.34958
11	3.933	344	0.67689	1.3437
12	0.84	389.4	0.67857	1.31345
13	0.706	328.9	0.71891	1.33193
14	2.756	368.2	0.68445	1.3605
15	3.832	390.9	0.66597	1.36639

16	3.597	316.8	0.73235	1.31597
17	2.622	357.6	0.74328	1.34202
18	3.798	313.8	0.69286	1.37899
19	1.849	341	0.66008	1.35462
20	0.303	253.3	0.70714	1.35294
21	2.017	378.8	0.7105	1.38487
22	2.218	242.7	0.73739	1.34034
23	0.101	272.9	0.72311	1.32269
24	3.664	295.6	0.68697	1.31849
25	0.269	318.3	0.74748	1.31513
26	1.647	233.6	0.66429	1.31176
27	3.462	383.4	0.73151	1.32185
28	1.311	297.1	0.67437	1.30336
29	3.126	244.2	0.69538	1.3
30	2.655	322.9	0.70042	1.4
31	0.336	327.4	0.72143	1.38908
32	2.387	386.4	0.67269	1.30504
33	1.143	262.4	0.74664	1.31933
34	1.109	250.3	0.65084	1.3521
35	1.782	229.1	0.70546	1.35546
36	1.345	324.4	0.68529	1.33361
37	2.689	268.4	0.72983	1.39832

	T = = = =	1		
38	3.966	276	0.68361	1.35042
39	1.681	359.2	0.7021	1.3084
40	3.63	248.7	0.73992	1.34454
41	0.504	241.2	0.72731	1.38992
42	3.261	331.9	0.65672	1.36723
43	2.118	397	0.72395	1.32437
44	1.445	338	0.72563	1.36218
45	0.202	279	0.6979	1.3916
46	1.378	356.1	0.7458	1.32353
47	0.034	260.8	0.67353	1.36303
48	0.235	335	0.66345	1.31681
49	3.092	257.8	0.74412	1.31092
50	0.067	300.2	0.73067	1.35882
51	3.361	298.7	0.65252	1.32857
52	3.731	371.3	0.73824	1.36555
53	2.017	342.5	0.66765	1.39328
54	0.908	256.3	0.69958	1.30672
55	2.824	398.5	0.71639	1.3563
56	1.546	351.6	0.65336	1.32101
57	0.471	266.9	0.65756	1.32017
58	3.294	362.2	0.67773	1.39412
59	1.21	380.3	0.70462	1.34286
60	2.084	245.7	0.71975	1.31008
61	1.748	330.4	0.69202	1.36891
62	0.773	224.5	0.69118	1.37983
63	2.151	236.6	0.67185	1.38151
64	1.076	347.1	0.69454	1.39916
65	3.025	223	0.70798	1.33277
66	3.866	269.9	0.71807	1.36975
67	1.983	232.1	0.7063	1.39244
68	2.252	265.4	0.68782	1.32521
69	1.95	286.6	0.65588	1.33109
70	2.42	350.1	0.74916	1.37731
71	1.244	280.5	0.71471	1.37395
72	2.487	325.9	0.67605	1.31429
73	4	259.3	0.07003	1.31765
74	0.975	220	0.72059	1.32773
75	2.723	307.7	0.68109	1.3479
76	1.882	291.1	0.65168	1.37479
77	2.992	263.9	0.6584	1.35798
78	2.319	339.5	0.70966	1.33697
79	3.697	353.1	0.66681	1.30924
80	0.874	251.8	0.65924	1.38824
81	1.176		0.03924	
82	0.807	306.2 247.2	0.74076	1.34622
83	3.496			1.35378
83	0.639	235.1 384.9	0.66176 0.71218	1.38655
85	1.008	363.7	0.71218	1.37647
86	1.58	283.5	0.68613	1.39496
87	0.672			
88		375.8	0.66513	1.34706
	3.193	393.9	0.6895	1.33025
89	0.941	294.1	0.74832	1.38319
90	3.395	254.8	0.69874	1.39664
91	0.571	309.2	0.66092	1.34874
92	3.563	310.8	0.7416	1.35042
93	2.185	221.5	0.67101	1.34538
94	2.353	288.1	0.73571	1.36471
95	0.437	333.4	0.69706	1.3042
96	2.555	277.5	0.70042	1.37143
97	1.277	304.7	0.72479	1.30252

98	1.613	400	0.73403	1.35966
99	0.168	289.6	0.68866	1.32941
100	0.403	319.8	0.69622	1.36134
101	0	360.7	0.6937	1.33529
102	2.454	348.6	0.73319	1.30168
103	2.857	227.6	0.72647	1.37059
104	2.79	271.4	0.66261	1.30084
105	3.765	345.5	0.71134	1.34118
106	3.227	226.1	0.69034	1.36387
107	1.042	366.7	0.74496	1.38571
108	0.538	381.8	0.72227	1.31261
109	1.916	395.5	0.67521	1.33782
110	2.958	292.6	0.66933	1.39076
111	2.924	365.2	0.65504	1.33613
112	3.529	315.3	0.73655	1.38739
113	0.134	369.7	0.67941	1.37815
114	2.286	303.2	0.73908	1.32605
115	0.739	230.6	0.68277	1.33445
116	2.588	301.7	0.70882	1.30588
117	3.429	238.2	0.67017	1.32689
118	3.328	354.6	0.70378	1.30756
119	3.059	285	0.71303	1.3395
120	1.815	321.3	0.72815	1.3958

#### Schedule B

## Optimal Latin hypercube design matrix calculation results

Sample	Head/	Eff	Sample	Head/	Eff
Points	(m)		Points	(m)	
1	5.012	0.7177	61	5.157	0.7132
2	6.496	0.6887	62	4.063	0.7198
3	4.06	0.7252	63	5.082	0.7036
4	6.721	0.6711	64	4.63	0.7212
5	4.037	0.7244	65	5.534	0.6856
6	6.487	0.6690	66	6.539	0.6733
7	4.097	0.7174	67	5.078	0.7067
8	4.339	0.7246	68	5.336	0.7032
9	5.808	0.6937	69	5.003	0.7077
10	4.037	0.7244	70	6.077	0.7042
11	6.487	0.6690	71	4.836	0.7210
12	4.097	0.7174	72	5.514	0.6986
13	4.339	0.7246	73	6.412	0.6675
14	5.808	0.6936	74	4.244	0.7167
15	6.338	0.6696	75	5.775	0.6958
16	6.623	0.6794	76	5	0.7100
17	6.109	0.6993	77	5.678	0.6888
18	6.593	0.6743	78	5.658	0.7034
19	4.982	0.7083	79	6.181	0.6718
20	3.829	0.7244	80	4.17	0.7218
21	5.459	0.7080	81	4.962	0.7222
22	5.395	0.7037	82	4.384	0.7227
23	3.723	0.7258	83	5.783	0.6778
24	6.299	0.6749	84	4.206	0.7229
25	4.026	0.7264	85	4.228	0.7171
26	4.608	0.7102	86	4.999	0.7159
27	6.527	0.6802	87	3.945	0.7204
28	4.583	0.7156	88	6.035	0.6837
29	5.727	0.6853	89	4.768	0.7254
30	5.969	0.6990	90	6.102	0.6819

Q. Xiang et al. / JAFM, Vol. 19, No. 1, pp. x-x, 2026.

31         4.072         0.7284         91         3.937         0.7234           32         5.309         0.6973         92         6.716         0.6810           33         4.745         0.7204         93         4.94         0.7013           34         4.27         0.7176         94         5.823         0.7047           35         4.879         0.7089         95         3.91         0.7230           36         4.72         0.7177         96         5.729         0.6995           37         5.953         0.6984         97         4.848         0.7199           38         6.406         0.6689         98         5.176         0.7134           39         5.025         0.7123         99         3.666         0.7246           40         6.252         0.6764         100         3.972         0.7255           41         4.058         0.7233         101         3.458         0.7210           42         5.991         0.6835         102         5.84         0.7011           43         5.467         0.7045         103         5.586         0.6900           44         5.1						
33         4.745         0.7204         93         4.94         0.7013           34         4.27         0.7176         94         5.823         0.7047           35         4.879         0.7089         95         3.91         0.7230           36         4.72         0.7177         96         5.729         0.6995           37         5.953         0.6984         97         4.848         0.7199           38         6.406         0.6689         98         5.176         0.7134           39         5.025         0.7123         99         3.666         0.7246           40         6.252         0.6764         100         3.972         0.7255           41         4.058         0.7233         101         3.458         0.7210           42         5.991         0.6835         102         5.84         0.7011           43         5.467         0.7045         103         5.586         0.6900           44         5.1         0.7190         104         5.512         0.6906           45         3.804         0.7269         105         6.655         0.6748           46         5.061		4.072	0.7284	91	3.937	0.7234
34         4.27         0.7176         94         5.823         0.7047           35         4.879         0.7089         95         3.91         0.7230           36         4.72         0.7177         96         5.729         0.6995           37         5.953         0.6984         97         4.848         0.7199           38         6.406         0.6689         98         5.176         0.7134           39         5.025         0.7123         99         3.666         0.7246           40         6.252         0.6764         100         3.972         0.7255           41         4.058         0.7233         101         3.458         0.7210           42         5.991         0.6835         102         5.84         0.7011           43         5.467         0.7045         103         5.586         0.6900           44         5.1         0.7190         104         5.512         0.6906           45         3.804         0.7269         105         6.655         0.6748           46         5.061         0.7181         106         5.643         0.6829           47         3.465	32	5.309	0.6973	92	6.716	0.6810
35         4.879         0.7089         95         3.91         0.7230           36         4.72         0.7177         96         5.729         0.6995           37         5.953         0.6984         97         4.848         0.7199           38         6.406         0.6689         98         5.176         0.7134           39         5.025         0.7123         99         3.666         0.7246           40         6.252         0.6764         100         3.972         0.7255           41         4.058         0.7233         101         3.458         0.7210           42         5.991         0.6835         102         5.84         0.7011           43         5.467         0.7045         103         5.586         0.6900           44         5.1         0.7190         104         5.512         0.6906           45         3.804         0.7269         105         6.655         0.6748           46         5.061         0.7181         106         5.643         0.6829           47         3.465         0.7233         107         4.838         0.7231           48         3.556	33	4.745	0.7204	93	4.94	0.7013
36         4.72         0.7177         96         5.729         0.6995           37         5.953         0.6984         97         4.848         0.7199           38         6.406         0.6689         98         5.176         0.7134           39         5.025         0.7123         99         3.666         0.7246           40         6.252         0.6764         100         3.972         0.7255           41         4.058         0.7233         101         3.458         0.7210           42         5.991         0.6835         102         5.84         0.7011           43         5.467         0.7045         103         5.586         0.6900           44         5.1         0.7190         104         5.512         0.6906           45         3.804         0.7269         105         6.655         0.6748           46         5.061         0.7181         106         5.643         0.6829           47         3.465         0.7233         107         4.838         0.7231           48         3.556         0.7205         108         4.068         0.7224           49         6.05	34	4.27	0.7176	94	5.823	0.7047
37         5.953         0.6984         97         4.848         0.7199           38         6.406         0.6689         98         5.176         0.7134           39         5.025         0.7123         99         3.666         0.7246           40         6.252         0.6764         100         3.972         0.7255           41         4.058         0.7233         101         3.458         0.7210           42         5.991         0.6835         102         5.84         0.7011           43         5.467         0.7045         103         5.586         0.6900           44         5.1         0.7190         104         5.512         0.6906           45         3.804         0.7269         105         6.655         0.6748           46         5.061         0.7181         106         5.643         0.6829           47         3.465         0.7233         107         4.838         0.7231           48         3.556         0.7205         108         4.068         0.7224           49         6.05         0.6874         109         5.004         0.7046           50         3.784 <td>35</td> <td>4.879</td> <td>0.7089</td> <td>95</td> <td>3.91</td> <td>0.7230</td>	35	4.879	0.7089	95	3.91	0.7230
38         6.406         0.6689         98         5.176         0.7134           39         5.025         0.7123         99         3.666         0.7246           40         6.252         0.6764         100         3.972         0.7255           41         4.058         0.7233         101         3.458         0.7210           42         5.991         0.6835         102         5.84         0.7011           43         5.467         0.7045         103         5.586         0.6900           44         5.1         0.7190         104         5.512         0.6906           45         3.804         0.7269         105         6.655         0.6748           46         5.061         0.7181         106         5.643         0.6829           47         3.465         0.7233         107         4.838         0.7231           48         3.556         0.7205         108         4.068         0.7224           49         6.05         0.6874         109         5.004         0.7046           50         3.784         0.7257         110         5.889         0.6908           51         5.912 </td <td>36</td> <td>4.72</td> <td>0.7177</td> <td>96</td> <td>5.729</td> <td>0.6995</td>	36	4.72	0.7177	96	5.729	0.6995
39         5.025         0.7123         99         3.666         0.7246           40         6.252         0.6764         100         3.972         0.7255           41         4.058         0.7233         101         3.458         0.7210           42         5.991         0.6835         102         5.84         0.7011           43         5.467         0.7045         103         5.586         0.6900           44         5.1         0.7190         104         5.512         0.6906           45         3.804         0.7269         105         6.655         0.6748           46         5.061         0.7181         106         5.643         0.6829           47         3.465         0.7233         107         4.838         0.7231           48         3.556         0.7205         108         4.068         0.7224           49         6.05         0.6874         109         5.004         0.7046           50         3.784         0.7257         110         5.889         0.6908           51         5.912         0.6799         111         5.649         0.6878           52         6.884<	37	5.953	0.6984	97	4.848	0.7199
40         6.252         0.6764         100         3.972         0.7255           41         4.058         0.7233         101         3.458         0.7210           42         5.991         0.6835         102         5.84         0.7011           43         5.467         0.7045         103         5.586         0.6900           44         5.1         0.7190         104         5.512         0.6906           45         3.804         0.7269         105         6.655         0.6748           46         5.061         0.7181         106         5.643         0.6829           47         3.465         0.7233         107         4.838         0.7231           48         3.556         0.7205         108         4.068         0.7224           49         6.05         0.6874         109         5.004         0.7046           50         3.784         0.7257         110         5.889         0.6908           51         5.912         0.6799         111         5.649         0.6878           52         6.884         0.6769         112         6.742         0.6821           53         5.238	38	6.406	0.6689	98	5.176	0.7134
41         4.058         0.7233         101         3.458         0.7210           42         5.991         0.6835         102         5.84         0.7011           43         5.467         0.7045         103         5.586         0.6900           44         5.1         0.7190         104         5.512         0.6906           45         3.804         0.7269         105         6.655         0.6748           46         5.061         0.7181         106         5.643         0.6829           47         3.465         0.7233         107         4.838         0.7231           48         3.556         0.7205         108         4.068         0.7224           49         6.05         0.6874         109         5.004         0.7046           50         3.784         0.7257         110         5.889         0.6908           51         5.912         0.6799         111         5.649         0.6878           52         6.884         0.6769         112         6.742         0.6821           53         5.238         0.7074         113         3.557         0.7217           54         4.305	39	5.025	0.7123	99	3.666	0.7246
42         5.991         0.6835         102         5.84         0.7011           43         5.467         0.7045         103         5.586         0.6900           44         5.1         0.7190         104         5.512         0.6906           45         3.804         0.7269         105         6.655         0.6748           46         5.061         0.7181         106         5.643         0.6829           47         3.465         0.7233         107         4.838         0.7231           48         3.556         0.7205         108         4.068         0.7224           49         6.05         0.6874         109         5.004         0.7046           50         3.784         0.7257         110         5.889         0.6908           51         5.912         0.6799         111         5.649         0.6878           52         6.884         0.6769         112         6.742         0.6821           53         5.238         0.7074         113         3.557         0.7217           54         4.305         0.7208         114         5.782         0.7055           55         6.025	40	6.252	0.6764	100	3.972	0.7255
43         5.467         0.7045         103         5.586         0.6900           44         5.1         0.7190         104         5.512         0.6906           45         3.804         0.7269         105         6.655         0.6748           46         5.061         0.7181         106         5.643         0.6829           47         3.465         0.7233         107         4.838         0.7231           48         3.556         0.7205         108         4.068         0.7224           49         6.05         0.6874         109         5.004         0.7046           50         3.784         0.7257         110         5.889         0.6908           51         5.912         0.6799         111         5.649         0.6878           52         6.884         0.6769         112         6.742         0.6821           53         5.238         0.7074         113         3.557         0.7217           54         4.305         0.7208         114         5.782         0.7055           55         6.025         0.6926         115         3.999         0.7200           56         4.62	41	4.058	0.7233	101	3.458	0.7210
44         5.1         0.7190         104         5.512         0.6906           45         3.804         0.7269         105         6.655         0.6748           46         5.061         0.7181         106         5.643         0.6829           47         3.465         0.7233         107         4.838         0.7231           48         3.556         0.7205         108         4.068         0.7224           49         6.05         0.6874         109         5.004         0.7046           50         3.784         0.7257         110         5.889         0.6908           51         5.912         0.6799         111         5.649         0.6878           52         6.884         0.6769         112         6.742         0.6821           53         5.238         0.7074         113         3.557         0.7217           54         4.305         0.7208         114         5.782         0.7055           55         6.025         0.6926         115         3.999         0.7200           56         4.621         0.7113         116         5.776         0.6984           57         3.77	42	5.991	0.6835	102	5.84	0.7011
45         3.804         0.7269         105         6.655         0.6748           46         5.061         0.7181         106         5.643         0.6829           47         3.465         0.7233         107         4.838         0.7231           48         3.556         0.7205         108         4.068         0.7224           49         6.05         0.6874         109         5.004         0.7046           50         3.784         0.7257         110         5.889         0.6908           51         5.912         0.6799         111         5.649         0.6878           52         6.884         0.6769         112         6.742         0.6821           53         5.238         0.7074         113         3.557         0.7217           54         4.305         0.7208         114         5.782         0.7055           55         6.025         0.6926         115         3.999         0.7200           56         4.621         0.7113         116         5.776         0.6984           57         3.772         0.7227         117         5.74         0.6773           58         6.1	43	5.467	0.7045	103	5.586	0.6900
46         5.061         0.7181         106         5.643         0.6829           47         3.465         0.7233         107         4.838         0.7231           48         3.556         0.7205         108         4.068         0.7224           49         6.05         0.6874         109         5.004         0.7046           50         3.784         0.7257         110         5.889         0.6908           51         5.912         0.6799         111         5.649         0.6878           52         6.884         0.6769         112         6.742         0.6821           53         5.238         0.7074         113         3.557         0.7217           54         4.305         0.7208         114         5.782         0.7055           55         6.025         0.6926         115         3.999         0.7200           56         4.621         0.7113         116         5.776         0.6984           57         3.772         0.7227         117         5.74         0.6773           58         6.193         0.6832         118         6.24         0.6815           59         4.64	44	5.1	0.7190	104	5.512	0.6906
47         3.465         0.7233         107         4.838         0.7231           48         3.556         0.7205         108         4.068         0.7224           49         6.05         0.6874         109         5.004         0.7046           50         3.784         0.7257         110         5.889         0.6908           51         5.912         0.6799         111         5.649         0.6878           52         6.884         0.6769         112         6.742         0.6821           53         5.238         0.7074         113         3.557         0.7217           54         4.305         0.7208         114         5.782         0.7055           55         6.025         0.6926         115         3.999         0.7200           56         4.621         0.7113         116         5.776         0.6984           57         3.772         0.7227         117         5.74         0.6773           58         6.193         0.6832         118         6.24         0.6815           59         4.647         0.7170         119         6.115         0.6899	45	3.804	0.7269	105	6.655	0.6748
48         3.556         0.7205         108         4.068         0.7224           49         6.05         0.6874         109         5.004         0.7046           50         3.784         0.7257         110         5.889         0.6908           51         5.912         0.6799         111         5.649         0.6878           52         6.884         0.6769         112         6.742         0.6821           53         5.238         0.7074         113         3.557         0.7217           54         4.305         0.7208         114         5.782         0.7055           55         6.025         0.6926         115         3.999         0.7200           56         4.621         0.7113         116         5.776         0.6984           57         3.772         0.7227         117         5.74         0.6773           58         6.193         0.6832         118         6.24         0.6815           59         4.647         0.7170         119         6.115         0.6899	46	5.061	0.7181	106	5.643	0.6829
49         6.05         0.6874         109         5.004         0.7046           50         3.784         0.7257         110         5.889         0.6908           51         5.912         0.6799         111         5.649         0.6878           52         6.884         0.6769         112         6.742         0.6821           53         5.238         0.7074         113         3.557         0.7217           54         4.305         0.7208         114         5.782         0.7055           55         6.025         0.6926         115         3.999         0.7200           56         4.621         0.7113         116         5.776         0.6984           57         3.772         0.7227         117         5.74         0.6773           58         6.193         0.6832         118         6.24         0.6815           59         4.647         0.7170         119         6.115         0.6899	47	3.465	0.7233	107	4.838	0.7231
50         3.784         0.7257         110         5.889         0.6908           51         5.912         0.6799         111         5.649         0.6878           52         6.884         0.6769         112         6.742         0.6821           53         5.238         0.7074         113         3.557         0.7217           54         4.305         0.7208         114         5.782         0.7055           55         6.025         0.6926         115         3.999         0.7200           56         4.621         0.7113         116         5.776         0.6984           57         3.772         0.7227         117         5.74         0.6773           58         6.193         0.6832         118         6.24         0.6815           59         4.647         0.7170         119         6.115         0.6899	48	3.556	0.7205	108	4.068	0.7224
51         5.912         0.6799         111         5.649         0.6878           52         6.884         0.6769         112         6.742         0.6821           53         5.238         0.7074         113         3.557         0.7217           54         4.305         0.7208         114         5.782         0.7055           55         6.025         0.6926         115         3.999         0.7200           56         4.621         0.7113         116         5.776         0.6984           57         3.772         0.7227         117         5.74         0.6773           58         6.193         0.6832         118         6.24         0.6815           59         4.647         0.7170         119         6.115         0.6899	49	6.05	0.6874	109	5.004	0.7046
52         6.884         0.6769         112         6.742         0.6821           53         5.238         0.7074         113         3.557         0.7217           54         4.305         0.7208         114         5.782         0.7055           55         6.025         0.6926         115         3.999         0.7200           56         4.621         0.7113         116         5.776         0.6984           57         3.772         0.7227         117         5.74         0.6773           58         6.193         0.6832         118         6.24         0.6815           59         4.647         0.7170         119         6.115         0.6899	50	3.784	0.7257	110	5.889	0.6908
53         5.238         0.7074         113         3.557         0.7217           54         4.305         0.7208         114         5.782         0.7055           55         6.025         0.6926         115         3.999         0.7200           56         4.621         0.7113         116         5.776         0.6984           57         3.772         0.7227         117         5.74         0.6773           58         6.193         0.6832         118         6.24         0.6815           59         4.647         0.7170         119         6.115         0.6899	51	5.912	0.6799	111	5.649	0.6878
54         4.305         0.7208         114         5.782         0.7055           55         6.025         0.6926         115         3.999         0.7200           56         4.621         0.7113         116         5.776         0.6984           57         3.772         0.7227         117         5.74         0.6773           58         6.193         0.6832         118         6.24         0.6815           59         4.647         0.7170         119         6.115         0.6899	52	6.884	0.6769	112	6.742	0.6821
55         6.025         0.6926         115         3.999         0.7200           56         4.621         0.7113         116         5.776         0.6984           57         3.772         0.7227         117         5.74         0.6773           58         6.193         0.6832         118         6.24         0.6815           59         4.647         0.7170         119         6.115         0.6899	53	5.238	0.7074	113	3.557	0.7217
56         4.621         0.7113         116         5.776         0.6984           57         3.772         0.7227         117         5.74         0.6773           58         6.193         0.6832         118         6.24         0.6815           59         4.647         0.7170         119         6.115         0.6899	54	4.305	0.7208	114	5.782	0.7055
57     3.772     0.7227     117     5.74     0.6773       58     6.193     0.6832     118     6.24     0.6815       59     4.647     0.7170     119     6.115     0.6899	55	6.025	0.6926	115	3.999	0.7200
58         6.193         0.6832         118         6.24         0.6815           59         4.647         0.7170         119         6.115         0.6899	56	4.621	0.7113	116	5.776	0.6984
59 4.647 0.7170 119 6.115 0.6899	57	3.772	0.7227	117	5.74	0.6773
	58	6.193	0.6832	118	6.24	0.6815
60 5.238 0.7061 120 5.493 0.7143	59	4.647	0.7170	119	6.115	0.6899
	60	5.238	0.7061	120	5.493	0.7143